Crystal Structure of Y34F Mutant Human Mitochondrial Manganese Superoxide Dismutase and the Functional Role of Tyrosine 34†,‡

ARTICLE *in* BIOCHEMISTRY · MARCH 1998

Impact Factor: 3.02 · DOI: 10.1021/bi972394l

10 AUTHORS, INCLUDING:

Gloria E O Borgstahl
University of Nebraska Medical Center
106 PUBLICATIONS **2,483** CITATIONS
SEE PROFILE

Harry Nick
University of Florida
126 PUBLICATIONS **4,117** CITATIONS
SEE PROFILE

John Tainer
University of Texas MD Anderson Cancer Center
457 PUBLICATIONS **30,025** CITATIONS
SEE PROFILE

Article

Crystal Structure of Y34F Mutant Human Mitochondrial Manganese Superoxide Dismutase and the Functional Role of Tyrosine 34

Yue Guan, Michael J. Hickey, Gloria E. O. Borgstahl, Robert A. Hallewell, James R. Lepock, Don O'Connor, Yunsheng Hsieh, Harry S. Nick, David N. Silverman, and John A. Tainer

Biochemistry, **1998**, 37 (14), 4722-4730• DOI: 10.1021/bi972394l • Publication Date (Web): 20 March 1998

Crystal Structure of Y34F Mutant Human Mitochondrial Manganese Superoxide Dismutase and the Functional Role of Tyrosine 34[†,‡]

Yue Guan,[§] Michael J. Hickey,[§] Gloria E. O. Borgstahl,[§] Robert A. Hallewell,[∥] James R. Lepock,[⊥] Don O'Connor,[○] Yunsheng Hsieh,[▽] Harry S. Nick,[▽] David N. Silverman,*[,▽] and John A. Tainer*[,§]

Department of Molecular Biology, The Scripps Research Institute, La Jolla, California 92037, Department of Biochemistry, Imperial College, London SW7 2A2, U.K., Departments of Pharmacology and Therapeutics and of Biochemistry and Molecular Biology, University of Florida, Gainesville, Florida 32610, Department of Physics, University of Waterloo, Waterloo, Ontario N2L 3G1, Canada, and Center for Fast Kinetic Research, University of Texas, Austin, Texas 78712

Received September 26, 1997; Revised Manuscript Received January 26, 1998

ABSTRACT: Tyrosine 34 is a prominent and conserved residue in the active site of the manganese superoxide dismutases in organisms from bacteria to man. We have prepared the mutant containing the replacement Tyr 34 → Phe (Y34F) in human manganese superoxide dismutase (hMnSOD) and crystallized it in two different crystal forms, orthorhombic and hexagonal. Crystal structures of hMnSOD Y34F have been solved to 1.9 Å resolution in a hexagonal crystal form, denoted as $Y34F_{hex}$, and to 2.2 Å resolution in an orthorhombic crystal form, denoted as $Y34F_{ortho}$. Both crystal forms give structures that are closely superimposable with that of wild-type hMnSOD, with the phenyl rings of Tyr 34 in the wild type and Phe 34 in the mutant very similar in orientation. Therefore, in Y34F, a hydrogen-bonded relay that links the metal-bound hydroxyl to ordered solvent (Mn−OH to Gln 143 to Tyr 34 to H_2O to His 30) is broken. Surprisingly, the loss of the Tyr 34 hydrogen bonds resulted in large increases in stability (measured by T_m), suggesting that the Tyr 34 hydroxyl does not play a role in stabilizing active-site architecture. The functional role of the side chain hydroxyl of Tyr 34 can be evaluated by comparison of the Y34F mutant with the wild-type hMnSOD. Both wild-type and Y34F had k_{cat}/K_m near 10^9 M^{-1} s^{-1}, close to diffusion-controlled; however, Y34F showed k_{cat} for maximal catalysis smaller by 10-fold than the wild type. In addition, the mutant Y34F was more susceptible to product inhibition by peroxide than the wild-type enzyme. This activity profile and the breaking of the hydrogen-bonding chain at the active site caused by the replacement Tyr 34 → Phe suggest that Tyr 34 is a proton donor for $O_2^{\bullet -}$ reduction to H_2O_2 or is involved indirectly by orienting solvent or other residues for proton transfer. Up to 100 mM buffers in solution failed to enhance catalysis by either Y34F or the wild-type hMnSOD, suggesting that protonation from solution cannot enhance the release of the inhibiting bound peroxide ion, likely reflecting the enclosure of the active site by conserved residues as shown by the X-ray structures. The increased thermostability of the mutant Y34F and equal diffusion-controlled activity of Y34F and wild-type enzymes with normal superoxide levels suggest that evolutionary conservation of active-site residues in metalloenzymes reflects constraints from extreme rather than average cellular conditions. This new hypothesis that extreme rather than normal substrate concentrations are a powerful constraint on residue conservation may apply most strongly to enzyme defenses where the ability to meet extreme conditions directly affects cell survival.

The respiratory chain in mitochondria is a major source of oxygen radicals, and mitochondrial manganese superoxide dismutase (*1*) protects mitochondria from oxidative damage by dismuting the superoxide into O_2 and H_2O_2. Structures of human mitochondrial superoxide dismutase (hMnSOD)[1] at 2.2 Å resolution (*2*) and at 3 Å resolution (*3*) reveal differences in assembly but subunit similarity to the bacterial MnSODs from *Bacillus stearothermophilus* at 2.4 Å (*4*) and *Thermus thermophilus* at 1.8 Å (*5*). The structure at 2.9 Å of FeSOD from *Pseudomonas ovalis* (*6*) and structure at 2.0 Å of FeSOD from *Mycobacterium tuberculosis* (*7*) also have a similar fold and active-site structure, including the same ligands and metal ion geometry. The active site of hMnSOD ligates the manganese with three histidines (His 26, 74, and 163), one aspartate (Asp 159), and a water molecule

[†] This work was supported by grants from the National Institutes of Health GM54903 (to D.N.S.), GM48495 (to J.A.T.), HL39593 (to H.S.N.), and F32CA69107 (to Y.G.).

[‡] Atomic coordinates have been deposited in the Brookhaven Protein Data Bank under accession codes 1AP5 for $Y34F_{ortho}$ and 1AP6 for $Y34F_{hex}$.

* Address correspondence to J.A.T. at MB4, The Scripps Research Institute, 10550 N. Torrey Pines Rd., La Jolla, CA 92037, or to D.N.S. at Department of Pharmacology and Therapeutics, University of Florida, Gainesville, FL 32610.

[§] The Scripps Research Institute.

[∥] Imperial College.

[⊥] University of Waterloo.

[○] University of Texas.

[▽] University of Florida.

[1] Abbreviations: MnSOD, manganese superoxide dismutase; hMnSOD, human manganese superoxide dismutase; Q143N MnSOD, mutant of manganese superoxide dismutase containing the replacement glutamine 143 → asparagine; Y34F MnSOD, mutant of manganese superoxide dismutase containing the replacement tyrosine 34 → phenylalanine; DSC, differential scanning calorimetry.

S0006-2960(97)02394-5 CCC: $15.00
Published on Web 03/20/1998

(hydroxyl anion) as the fifth ligand in a trigonal bipyramidal arrangement (*2*). The hMnSOD is a homotetramer (*2*, *8*, *9*) that is more compact than the structures of the bacterial MnSODs as indicated by the shorter distances between metals in the individual subunits (*2*). The tetrameric structure of hMnSOD forms a ring of positive electrostatic charge surrounding the active sites to enhance attraction of substrate (*2*) similar to that observed in Cu/ZnSOD and mutants (*10*).

The metal in Mn superoxide dismutases cycles between oxidized and reduced states:

$$Mn^{3+} + O_2^{\bullet -} \underset{k_{-1}}{\overset{k_1}{\rightleftarrows}} [Mn^{3+}{-}O_2^{\bullet -}] \xrightarrow{k_2} Mn^{2+} + O_2 \quad (1)$$

$$Mn^{2+} + O_2^{\bullet -} \underset{k_{-3}}{\overset{k_3}{\rightleftarrows}} [Mn^{2+}{-}O_2^{\bullet -}] + 2H^+ \underset{k_{-4}}{\overset{k_4}{\rightleftarrows}} Mn^{3+} + H_2O_2 \quad (2)$$

Initial studies of the MnSOD from *B. stearothermophilus* determined that its catalysis is complicated by the presence of an inactive form of the enzyme that can interconvert to an active form, but these studies did not designate the nature of the inactive form (*11*, *12*). Steady-state constants for catalysis by MnSOD from *T. thermophilus* were obtained by Bull et al. (*13*) from stopped-flow experiments and for the hMnSOD using both stopped-flow and pulse radiolysis (*8*). In both studies, the rapid emergence of the inactive form of the enzyme was demonstrated. Bull et al. (*13*) observed the inactive form spectrophotometrically during steady state, and they suggested that the inactive form results from oxidative addition of $O_2^{\bullet -}$ to the Mn(II) form of the enzyme, resulting in a side-on peroxo complex of Mn(III).

Here we have examined the function of the active-site residue Tyr 34, which is close to the manganese but not a ligand of this metal. Tyr 34 is evidently critical structurally or functionally as it is conserved in all of the eukaryotic and bacterial MnSODs reported to date and in the bacterial FeSODs as well. Tyr 34 forms a hydrogen-bond network that includes Gln 143 and the metal−ligand cluster, and the properties of this tyrosine may be linked to catalysis at the metal ion. The amide group of Gln 143 (Nϵ2) is 4.6 Å from the manganese and 2.7 Å from the hydroxyl group of Tyr 34 to which it hydrogen-bonds (*2*). In the complex of azide with Mn(III)SOD from *T. thermophilus*, the azide is a Mn ligand and forms a hydrogen bond to the hydroxyl group of Tyr 34 (*14*), which suggests by analogy a potential binding mode for superoxide. Recent reports on catalytic activity of *Escherichia coli* Y34F FeSOD mutant suggest that Tyr 34 is multifunctional and essential for maximal activity of FeSOD (*15*, *16*).

We have replaced Tyr 34 with Phe, determined two independent crystal structures including the highest resolution hMnSOD structure to date, defined the thermostability, and measured the catalytic properties of the resulting mutant Y34F hMnSOD. This replacement caused minimal alteration of the active-site structure compared with the wild type, increased thermostability, and allowed us to test the functional role of the side-chain hydroxyl of Tyr 34 in catalysis. We observed a decrease in the maximal catalytic rate of superoxide decay (k_{cat}) by an order of magnitude for the mutant Y34F compared with the wild type. However, the values of k_{cat}/K_m for both enzymes were similar at 10^9 M^{-1} s^{-1}, near diffusion-controlled. The mutant Y34F exhibits rapid product inhibition qualitatively similar to the wild-type MnSOD; however, the magnitude of this inhibition was significantly greater in the mutant. These features provide new information on the hMnSOD catalytic mechanism, possible roles of Tyr 34 in proton-transfer pathways, and the evolutionary conservation of active-site residues in metalloenzymes.

MATERIALS AND METHODS

PCR-Based Site-Directed Mutagenesis. The oligonucleotides GCATATGAAGCACAGCCTCC and GGAGATCTCAGCATAACGATC were used as primers for PCR to amplify the hMnSOD cDNA [cDNA sequence reported by Beck et al. (*17*)]. The plasmid pHMNSOD4 (ATCC 59947), which encodes hMnSOD, was subcloned into the TA cloning vector, pCRII (Invitrogen Corp.). Four primers were designed and used for PCR-based site-directed mutagenesis to create the mutant Y34F hMnSOD. First we designed a pair of oligonucleotides, primers 1 (5′ GCAGCTTACTGTATTCTGCAG 3′) and 2 (5′ CCTTTAAACACAGCCTCCCCG 3′), which through PCR recreate the entire MnSOD coding region flanking the mutation. In addition we prepared two oligonucleotides, designated as primers 3 (5′ CCACGCGGCCTTCGTTAACAACCTG 3′) and 4 (5′ CAGGTTGTTAACGAAGGCCGCGTGG 3′), whose sequences were complementary to each other and contained the mutation of interest. Two separate PCR reactions were used to amplify the 5′ portion (primers 1 and 4) and 3′ portion (primers 3 and 2) of the MnSOD cDNA. The PCR products from these two reactions were purified by electroelution and used as template DNA for the second round of PCR using primers 1 and 2. The Y34F hMnSOD PCR product was cloned into the TA cloning vector (pCRII) and subsequently subcloned into the expression vector pTrc 99A (Pharmacia Corp.). The subcloning was accomplished by using the restriction sites, *Dra*I and *Pst*I, incorporated into primers 1 and 2, respectively. The *Dra*I site, which corresponds to the N-terminal portion of the protein, was annealed to the *Nco*I site in pTrc 99A, recreating an ATG codon, whereas the C-terminal end of the cDNA was annealed to the *Pst*I site of the vector. The mutation, along with the remainder of the coding sequence, was verified by DNA sequencing. This construct expressed hMnSOD in the mutant *SodA*$^-$/*SodB*$^-$ *E. coli* (strain QC 774) as a mature protein tagged with an extra Met at the amino terminus. Culture conditions included additional supplementation by 5 mM $MnCl_2$. Yields of MnSOD mutant protein were on average 50 mg of protein/50 g of bacterial pellet.

Purification of Human MnSOD. The mutant Y34F hMnSOD used in kinetic and spectroscopic studies was purified from *E. coli* using a combination of heat treatment (60 °C) and ion-exchange chromatography (DE52 and CM52) according to the procedures of Beck et al. (*18*). The purity of the resulting samples was determined on SDS−polyacrylamide gels, which showed one intense band. The purified enzyme was dialyzed extensively against EDTA and a portion of the resulting protein was digested with nitric acid for manganese analysis by atomic absorption spectrometry (Perkin-Elmer 5100PC). These measurements were used to determine the concentration of enzyme.

Crystallography. Mutagenesis, expression, and purification for crystallization was done as described previously (*19*). The orthorhombic crystals were grown from solutions consisting of 10 mg/mL protein buffered in 25 mM potassium phosphate at pH 7.8 and 20% poly(ethylene glycol) (PEG) 4000. These needle-shaped crystals grew after 7 days and belong to space group $P2_12_12$ with unit cell dimensions of $a = 75.2$ Å, $b = 79.8$ Å, and $c = 68.8$ Å. Initial data were collected on a Siemens Xentronics area detector and rotating-anode X-ray generator to 2.8 Å resolution. The initial structure refinement of the mutant model derived from the isomorphous wild-type enzyme coordinates (*2*) was performed using the simulated annealing (SA) method in X-PLOR (*20*). High-resolution 2.4 Å data were later collected at the Stanford Synchrotron Radiation Laboratory (SSRL). The data were processed using DENZO (*21*) and the R_{sym} was 7.5%. The data are 94.5% complete. After several cycles of refinement, the model was rebuilt to σ_A-weighted $2F_o - F_c$ and $F_o - F_c$ omit maps (*22*) using XFIT (*23*). The refinement against these data was completed in X-PLOR using the bulk solvent correction (*24*) with the manganese ion completely unrestrained during the final round of refinement to remove any force field bias. The final model consists of two Y34F MnSOD subunits and 252 solvent waters with an *R*-factor of 18.6% and R_{free} of 26.9%.

Large, hexagonal crystals of Y34F, nonisomorphous to those of wild-type hMnSOD, were grown from Na_2KPO_4 at pH 7.0. Hexagonal crystals belonged to space group $P6_122$, with unit cell dimensions of $a = b = 80.9$ Å and $c = 242.5$ Å. Initial data were collected on the MAR image plate area detector to 2.8 Å resolution. A 1.9 Å resolution data set was then collected on the translated MAR image plate at the Protein Structure Facility at the University of California, San Diego. A total of five crystals were used to collect the complete data set. The data were processed using DENZO and the R_{sym} was 7.7% after scaling the data from five different crystals with 88% completeness to 1.9 Å resolution. The structure of the hexagonal form was eventually solved with AMoRe (*25*) using one monomer of MnSOD as a probe. The SA refinement using the X-PLOR package converged to an *R*-factor of 23%. The model was refit to SA-omit (*20*) and σ_A-weighted $F_o - F_c$ (*22*) maps. The solvent molecules were located by using the program PICK (*26*) and examined in σ_A-weighted $F_c - F_c$ omit maps. The final *R*-factor converged to 18.2% (R_{free} of 23.6%) with 358 water molecules (Table 1). The average temperature factor *B* value for the protein atoms is 25.4 Å^2. The final model includes two Y34F MnSOD subunits in the asymmetric unit with the active site well-defined by the $2F_o - F_c$ electron density map (see Figure 1). The $Y34F_{ortho}$ data were collected at room temperature and the $Y34F_{hex}$ data were collected at 10 °C. Atomic coordinates have been deposited in the Brookhaven Protein Data Bank under accession codes 1AP5 for $Y34F_{ortho}$ and 1AP6 for $Y34F_{hex}$.

Differential Scanning Calorimetry. A Microcal-2 high-sensitivity differential scanning calorimeter was used to obtain all denaturation profiles. The human MnSOD and mutant protein at 2.4−3.2 mg/mL in 2 mM potassium phosphate buffer (pH 7.8) were deaerated under mild vacuum for 5 min and immediately scanned at a rate of temperature increase of 1 °C/min. The baseline and change in specific heat (ΔC_p) upon denaturation were corrected as previously described (*19*). The peaks of the differential scanning calorimetry profile were deconvoluted assuming a reversible, non-two-state model (*27*) and using the software package ORIGIN (Microcal, Inc.). ΔH, ΔS, and T_m, defined as the temperature of half-completion, for each transition were obtained from the best fits.

Table 1: Diffraction Data and Refinement Statistics for $Y34F_{ortho}$ and $Y34F_{hex}$ MnSODs

crystal form	$P2_12_12$	$P6_122$
resolution (Å)	2.4	1.9
total observations	51722	130874
unique reflections	15865	35261
completeness of data (%)	94.5	88.3
$\langle F \rangle > 2\sigma$ (%)	92.8	87.6
R_{sym}[a] (%)	7.5	7.7
$<I/\sigma I>$	20.0	13.7
R (%)	18.6	18.2
R_{free}[b]	26.9	23.6
no. of atoms	3400	3507
no. of water molecules	252	358
rmsd bonds (Å)	0.009	0.008
rmsd angles (deg)	1.4	1.4

[a] R_{sym} is the unweighted *R* value on *I* between symmetry mates. [b] R_{free} is the *R* factor of 5% randomly selected reflections never used in refinement.

Pulse Radiolysis. These experiments were carried out at the Center for Fast Kinetics Research at the University of Texas at Austin using a 4-Mev van der Graaff accelerator. A single high-dose electron pulse was used to generate superoxide radical anions from oxygen in aqueous solutions containing 10 mM sodium formate as hydroxyl radical scavenger (*28*) and 50 μM EDTA in addition to buffer and enzyme. All pulse radiolysis experiments were carried out at 20 °C. The dismutation of $O_2^{\bullet -}$ was followed spectrophotometrically from an absorbance band centered at 250 nm [$\epsilon = 2000$ M^{-1} cm^{-1} (*29*)] using a cell with a path length of 2.5 cm. Progress curves for each set of 6−9 experiments were averaged. Exposure to ultraviolet radiation was minimized by opening a mechanical shutter a fraction of a second before each pulse.

RESULTS AND DISCUSSION

Mutant Enzyme Structure and Active-Site Geometry. The Y34F structure and active-site geometry is well-defined by the 1.9 Å electron density maps (Figure 1). The three-dimensional structure of the Y34F human MnSOD mutant is similar to that of the wild-type hMnSOD; each is a homotetramer in which subunits A and C (A and B in $Y34F_{ortho}$) form the asymmetric unit (Figure 2A). The subunit consists of two structural domains: an N-terminal helical hairpin domain consisting of two long antiparallel α helices separated by a tight turn and a C-terminal α/β domain, containing a central three-stranded antiparallel β sheet and five α helices (Figure 2B). The two domains are joined by the active-site manganese, which is liganded to three histidines, one aspartate, and one hydroxyl group (Figure 2C). The structures are well refined with almost all $\phi-\psi$ angles in the energetically preferred regions in a Ramachandran plot (*30*). Residues 142 and 170 are consistent outliers in MnSOD structures, including the wild-type structure, indicating an unusual type of tight turn. The 1.9 Å resolution data for Y34F provides the most accurate and highest resolution hMnSOD structure to date.

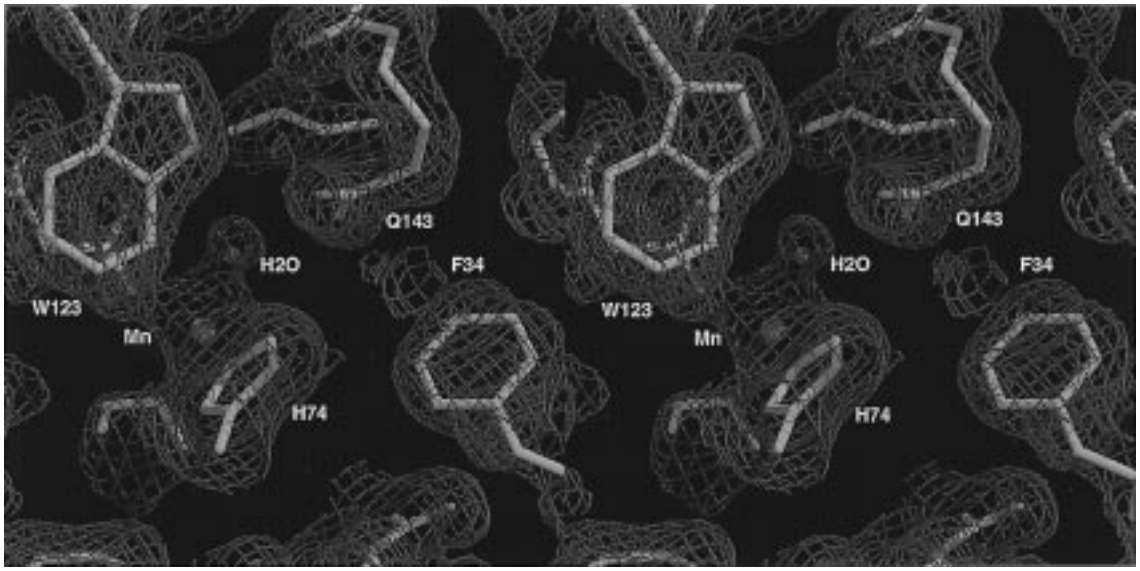

FIGURE 1: Diagram showing the active site of the Y34F mutant of MnSOD (hexagonal crystal form) in its $2F_o - F_c$ electron density (1σ blue contours). The structure has been refined to 1.9 Å resolution with F34 and Q143 in good density.

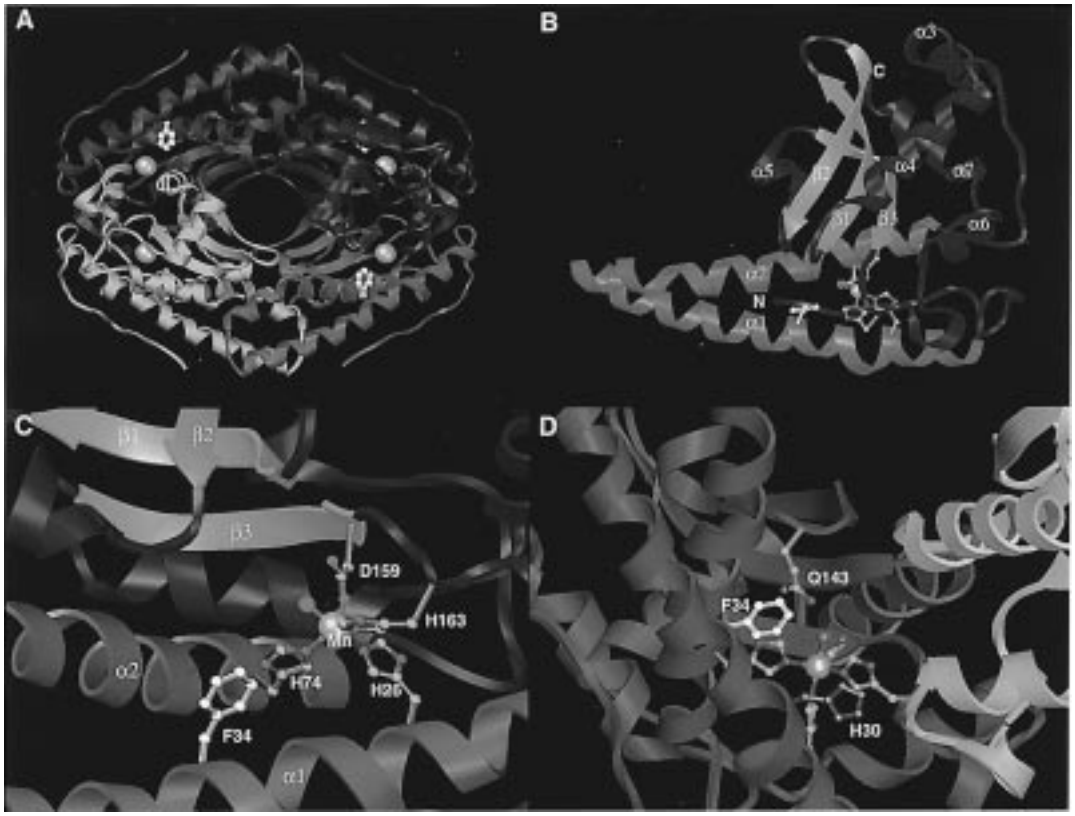

FIGURE 2: hMnSOD Y34F tetrameric structure, subunit fold, and active-site structure rendered as Ribbons diagrams (38). (A) Tetramer. Individual subunits are colored: A, yellow; B, green; C, magenta; and D, blue. Manganese ions are shown as pink spheres and the side chains of Phe34 are shown in white ball-and-stick representation. The A/B and C/D dimers (A/C and B/D in $Y34F_{hex}$) each form a crystallographic asymmetric unit. (B) Subunit fold. The Y34F MnSOD subunit is colored to emphasize secondary structure and domain organization. The N-terminal domain (bottom) is made up of the N-terminal loop (blue) and two long α helices (α1 and α2) (pink). The C-terminal α/β domain (top) is composed of five α helices (α3−α7) (blue) and three β strands (β1−β3) (orange). The pink-colored manganese lies between the two domains. (C) Active site geometry. The trigonal bipyramidal geometry of the five manganese ligands and Phe34 are drawn in a ball-and-stick representation. Amino acids from both domains contribute to the active site. (D) Active-site channel. The channel is formed for each subunit by residues from both subunits of the asymmetric unit. The superoxide substrate may pass through this channel to reach the Mn(III) ion. Residues that lie between the channel and Mn(III) ion are shown in ball-and-stick representation.

For each of the four active sites within the hMnSOD tetramer, a channel made up of amino acid residues primarily from two subunits provides the most probable access for the superoxide substrate to the catalytic Mn(III) ion. This deep channel is shaped like a lopsided funnel about 34 Å wide at the mouth between Lys 51A and Lys 178B and 8 Å wide at the base between Tyr 34A and Arg 173B. The channel funnel is lopsided by having sides ranging from 14 to 31 Å in depth. This funnel appears suitable for electrostatic guidance of superoxide anion as it is lined by eight lysines

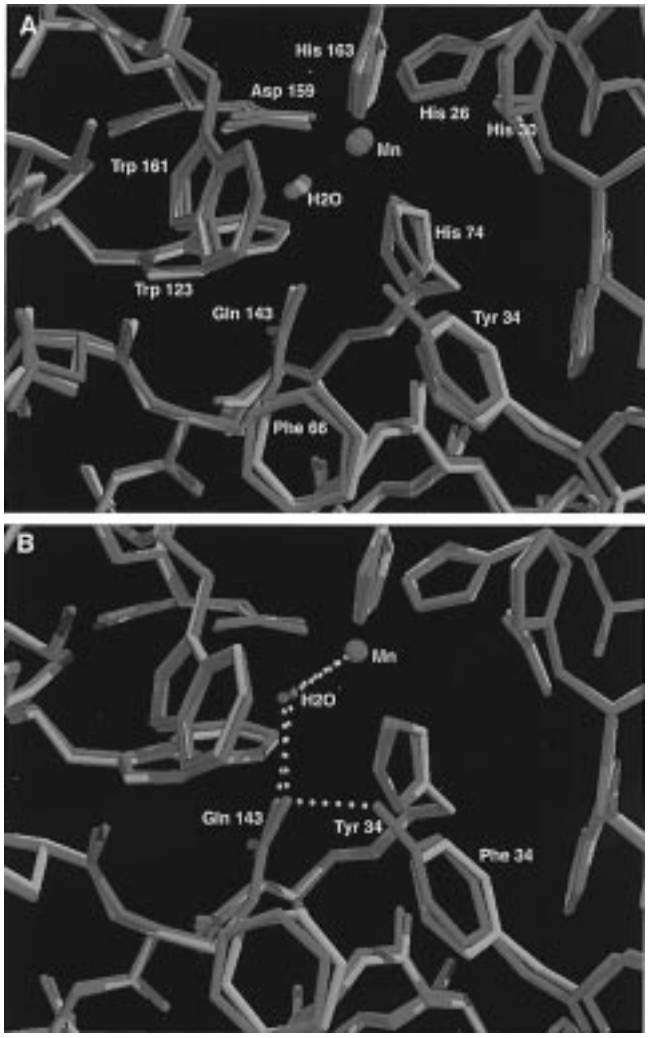

FIGURE 3: (A) Diagrams comparing the geometry of the active site in the native MnSOD and Y34F MnSOD in two crystal forms. The native is shown in blue, $Y34F_{ortho}$ in pink, and $Y34F_{hex}$ in yellow. Positions of Mn ligands and Gln143 are slightly shifted. (B) Diagram showing the hydrogen-bonding scheme of the native MnSOD (blue) and $Y34F_{ortho}$ (multicolored). Phe34 cannot form a hydrogen bond to Nϵ2 of Gln143.

from three subunits: 29A, 44A, 51A, 106B, 108B, 110B, 178B, and 130C. Arg 173, His 30, Gly 120, and Tyr 34 form the base of the funnel. The side chains of Tyr 34, His 30, and Gln 143 gate the Mn-bound water ligand from the channel solvent (Figure 2D).

Structural Comparison of the Y34F Mutant and the Wild Type. Superposition of the wild-type (*2*) and Y34F subunit structures reveals close structural similarity, with a root-mean-square deviation for 196 Cα atoms of 0.29 and 0.26 Å for the orthorhombic and hexagonal crystal forms, respectively. In the vicinity of the manganese, the positions of the three histidine ligands (26, 74, and 163), Asp 159, Gln 143, and the OH^-/H_2O are only slightly shifted compared to the wild-type protein (Figure 3A). The imidazole ring of His 74 in $Y34F_{ortho}$ (the orthorhombic crystal form) subunit A is rotated about 20° (10° in subunit B) relative to that in the wild-type and $Y34F_{hex}$ (the hexagonal crystal form). However, the superior 1.9 Å resolution and 23.6% R_{free} for the Y34F hexagonal form argue that the active-site ligands are virtually identical to those of the wild-type enzyme. The superposition of the tetramers of the two crystal forms shows

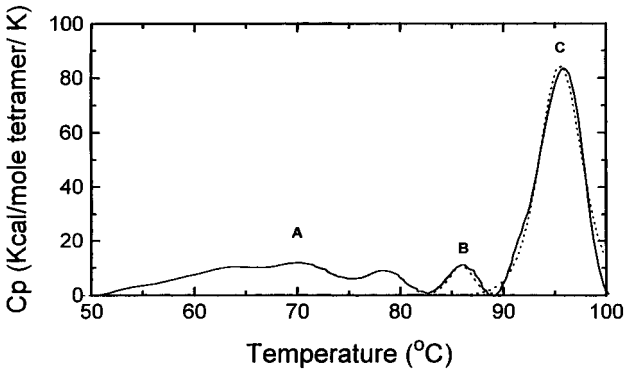

FIGURE 4: Differential scanning calorimetry profiles of apparent excess specific heat (C_p) vs temperature for Y34F hMnSOD. The dotted lines are the best fits to the individual components of the experimental profile (solid lines). Comparable experiments on wild-type hMnSOD are given in Borgstahl et al. (*19*).

no difference in orientation. The averaged Mn−His Nϵ2 distances in the Y34F mutant (2.12 Å in $Y34F_{ortho}$ and 2.13 Å in $Y34F_{hex}$) are slightly longer than in the wild-type (2.09 Å). Consistent results are also observed for the Mn−Asp Oδ1 distances (2.09 Å in $Y34F_{ortho}$ and 1.97 Å in $Y34F_{hex}$ and 1.94 Å in the wild type), representing slightly expanded coordination geometry. The OH^-/H_2O ligand in $Y34F_{hex}$ is about the same distance from the Mn ion as seen in the wild-type enzyme, suggesting that both mutant and the wild-type enzymes have a similar hydroxyl ligand at this position. The ligand OH^-/H_2O $Y34F_{ortho}$ has very weak electron density and a high *B*-factor (47 $Å^2$ in comparison with 17 $Å^2$ in $Y34F_{hex}$ and 22 $Å^2$ in native), so this OH^-/H_2O is less well defined in this orthorhombic crystal form. This is surprising as this structure was solved from crystals grown at a slightly higher pH (pH 7.8) than the wild-type crystals (pH 7.5) and $Y34F_{hex}$ (pH 7.0). The decreased occupancy of the water site in the $Y34F_{ortho}$ crystal form does not affect the coordination geometry of the other ligands and is consistent with this being an exchangeable site suitable for superoxide binding. Superposition of the two different crystal forms of Y34F mutants reveals an rmsd of 0.3 Å for 196 Cα atoms. Apparently the crystal packing did not change the overall structure significantly. Each of the two subunits in the asymmetric unit of the Y34F mutant (two crystal forms) can be superimposed with another subunit in the wild-type structure with rmsd for 196 Cαs in the range of 0.19−0.40 Å, representing very similar three-dimensional structures. In the native enzyme, the hydroxyl group of Tyr 34 forms a hydrogen bond to the amide moiety of Gln 143 (2.7 Å in distance); this interaction is absent in the mutant structure due to the missing hydroxyl group (Figure 3B). Therefore, the single, most significant structural change in Y34F compared to the wild-type enzyme is the breaking of the Tyr34−Gln143−H_2O−Mn hydrogen-bonding chain in the mutant.

Thermal Stability. The thermal stability of human Y34F MnSOD was determined by differential scanning calorimetry (DSC). Five peaks were resolvable for Y34F MnSOD (Figure 4), three overlapping small ones (labeled A) with T_ms ∼ 63, 71, and 78 °C, another small peak labeled B with T_m 86 °C, and a much larger one (labeled C) with T_m 96 °C. This notation for labeling the transitions was chosen to correspond to that used previously for native and I58T MnSOD (*19*). Transition C is the main unfolding transition

Table 2: Thermodynamic Parameters for Reversible Unfolding of MnSOD

enzyme	component	T_m (°C)	ΔH^a (kcal/mol)	$\Delta\Delta G^{a,b}$ (kcal/mol)	$\Delta\Delta G^{*\,c}$ (kcal/mol)
native	B	70	142	0	0
native	C	88.9	90.6	0	0
Y34F	B	85.9	351	15.5	12.7
Y34F	C	95.6	197	3.5	3.1

[a] ΔH and ΔG are given per mole of tetramer. [b] $\Delta\Delta G$ is ΔG of the mutant calculated at the appropriate T_m of the native, assuming constant ΔH ($\Delta C_p = 0$). [c] $\Delta\Delta G^*$ was calculated assuming $\Delta C_p = 0.12$ cal/g.

of the enzyme. Surprisingly, Y34F is more stable than native MnSOD, with increases of 16 °C in T_m (B) and 6.7 °C in T_m (C). The identity of transitions A and B are unknown; however, the T_m of transition B corresponds to the thermal inactivation temperature (*19*). Thus, this transition, which occurs with a relatively small absorption of heat, results in an inactive enzyme. Transition A, which is not observed in native MnSOD, appears to have multiple components in I58T and Y34F MnSOD and is extremely weak and nearly undetectable in Q143N MnSOD (*31*). From the I58T mutant this transition has no effect on activity (*19*).

The estimated stabilization of the mutant compared to native, given as $\Delta\Delta G$, was calculated from the thermodynamic parameters ΔH, ΔS, and T_m (Table 2). A reversible analysis of an apparently irreversible process is possible if there is little accumulation of the irreversibly denatured species during that part of the DSC scan used for analysis (*27*). Irreversible species will accumulate near the high-temperature end of each transition; therefore, to minimize errors in determining ΔH and ΔS, the high-temperature end was excluded in the reversible curve-fitting (*32*). As expected for an irreversible transition, the high-temperature end of the DSC profiles are not fit well with the reversible model (Figure 4) because of the sharp drop in the C_p above the T_m of peak C, which is a consequence of irreversibility (32). To reduce this fitting problem, peak C was fit with the high-temperature tail (beyond the peak half-height on the downslope) excluded (Figure 4). Due to irreversibility, an accurate value for ΔC_p is unobtainable, so $\Delta\Delta G$ was calculated by two procedures: (1) by assuming constant ΔH and ΔS and (2) by estimating the temperature dependence of ΔH and ΔS using a value of 0.12 cal/g for ΔC_p, which is an average value for several small, globular proteins (*33*). These methods give a stabilization $\Delta\Delta G$ of 13−16 kcal/mol for transition B and 3.1−3.5 kcal/mol for transition C (Table 2). The magnitude of $\Delta\Delta G$ for transition B is greatly affected by the large value of ΔH for transition B, which is more than twice that for transition B of native MnSOD.

The surprisingly great stabilization resulting from the Y34F mutation indicates that the Tyr 34 hydrogen-bonded network does not stabilize the active-site architecture. Instead, the increased stability of Y34F suggests that the conservation of tyrosine at residue 34 reflects a functional optimization. These results are consistent with detailed studies on the catalytic residues of T4 lysozyme, which have supported the general theory that enzyme residues involved in function are not optimized for stability (*34*). However, our results on the structure, stability, and thermostability of Y34F hMnSOD differ from an analysis on the Y34F mutation on *E. coli* Fe superoxide dismutase where activity and thermal inactivation

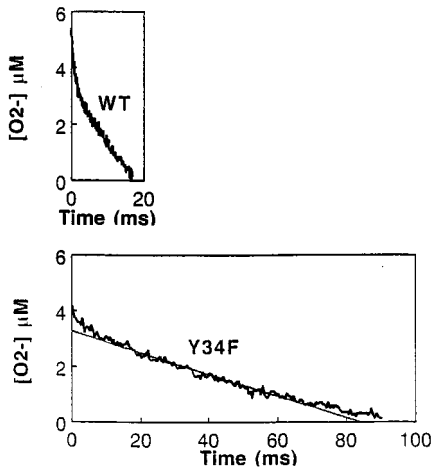

FIGURE 5: Comparison of superoxide decay catalyzed by (top) wild-type human MnSOD and (bottom) Y34F human MnSOD as determined by pulse radiolysis. Data show the decrease in superoxide as determined from its absorbance at 250 nm ($\epsilon = 2000\ M^{-1}\ cm^{-1}$). The solutions contained 0.5 μM wild-type MnSOD or 0.5 μM Y34F MnSOD, 50 μM EDTA, 10 mM sodium formate, and 2.0 mM sodium pyrophosphate at pH 9.6 and 20 °C.

results were interpreted to suggest roles for Tyr 34 in both stability and catalysis (*15*).

Catalytic and Spectroscopic Features of Y34F Human MnSOD. The general features of catalysis by Y34F hMnSOD are qualitatively similar to those of catalysis by wild-type hMnSOD; there is an initial burst of activity followed by a region of much slower zero-order decay of superoxide (Figure 5). The initial burst was evident in the first millisecond of catalysis and detected using pulse radiolysis. The zero-order region is interpreted for both *T. thermophilus* MnSOD (*13*) and hMnSOD (*8*) as a region of inhibition caused most likely by the binding of product peroxide to MnSOD. The zero-order rate constant in this inhibited region for the Y34F mutant is smaller by about 4-fold than that of the wild-type hMnSOD under comparable conditions suggesting that the extent of inhibition is greater for the mutant.

This conclusion is supported by the smaller size of the initial burst of activity catalyzed by Y34F MnSOD compared to the wild-type (Figure 5). The amplitude of this burst represents catalytic decay of superoxide before the onset of the zero-order region of inhibition. The magnitude of this burst (micromolar of $O_2^{\bullet -}$) as a function of enzyme concentration (micromolar) had a slope of approximately 2 (data not shown), indicating that superoxide consumed in this initial burst is not stoichiometric with enzyme concentration and that multiple turnovers occur before the enzyme becomes inhibited. The slope of a similar plot for the wild-type hMnSOD under comparable conditions is 12, indicating that the wild-type enzyme is less inhibited and undergoes more catalytic cycles before inhibition than does Y34F MnSOD. In the wild-type hMnSOD this region of zero-order catalysis has a solvent hydrogen isotope effect from 2.2 to 3.1 depending on conditions, indicating a role for proton transfer in the steps by which the product is released from the inhibited enzyme (*8*). We do not observe any enhancement of this zero-order region of the catalysis by either wild type or Y34F upon increasing the concentration of the following buffers from 2 to 100 mM: glycine (at pH 9.6), ethanolamine (pH 10.0), and carbonate (pH 10.3).

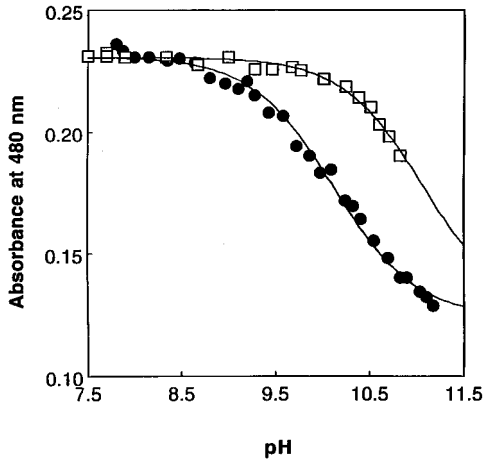

FIGURE 6: Absorbance at 480 nm as a function of pH for Y34F human manganese superoxide dismutase (□) and the wild-type human MnSOD (●) at 20 °C. The solid line for wild type is a fit to a single ionization with a pK_a of 10.1 ± 0.1; for Y34F MnSOD the value is pK_a = 11.1 ± 0.1.

Hence, this product inhibition cannot be overcome by donation of protons from these buffers in solution.

The visible absorption spectrum of Y34F hMnSOD displayed a maximum at 480 nm with a shoulder at 600 nm, similar to published spectra of the oxidized form of the wild-type enzyme (*8*, *13*, *18*). Accordingly, the Y34F mutant was purified predominantly in the oxidized form, although we recognize that are dealing with enzyme with mixed oxidation states of Mn^{2+} and Mn^{3+}. The pH dependence of this absorbance for Y34F hMnSOD can be described by a single ionization with pK_a near 11; for the wild-type enzyme this pK_a was closer to 10 (Figure 6). There is evidence of enzyme denaturation above pH 11. An ionization of pK_a near 9 is observed for wild-type FeSOD, describing the pH dependence of K_m and the binding of azide, among other properties (*35*). This pK_a is believed to be caused by the addition of an hydroxide ligand to the metal in the ferric form; the pK_a near 9 in the ferrous form is believed to be the ionization of Tyr 34 (*14*). From the crystal structure results, the replacement Tyr 34 → Phe has destroyed the hydrogen-bonding network involving this residue, Gln 143 and the metal-bound water; this is consistent with a destabilization of metal-bound hydroxide and hence an increase in the pK_a and lower activity for Y34F. This suggestion is also supported by examination of spectral properties and azide inhibition of MnSOD from *E. coli* in comparison with FeSOD and iron-substituted MnSOD (*36*).

Catalytic Mechanism of Y34F Human MnSOD. The kinetic mechanism of Scheme 1 used to describe the wild-type MnSOD (*8*, *13*) can also describe catalysis by Y34F MnSOD (Figure 7), as shown by pulse radiolysis. The fit was obtained using KINSIM (*37*), and the rate constants for Y34F MnSOD obtained in this manner are given in Table 3, where they are compared with the constants found for the wild-type hMnSOD under comparable conditions. In this simulation, the breakdown of the enzyme−substrate complex for enzyme in the reduced state, represented by k_{-3} in Scheme 1, is much slower for Y34F compared with the wild type, whereas the values of k_3 are the same for both enzymes (Table 3). This indicates a longer lifetime for this complex and hence a greater probability it will form the inhibited complex, which is confirmed by simulations of the catalysis using the data of Table 3 and KINSIM. The rate constants in Y34F for actual formation of the dead-end complex itself,

Scheme 1

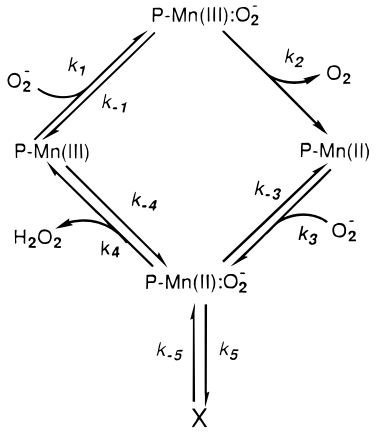

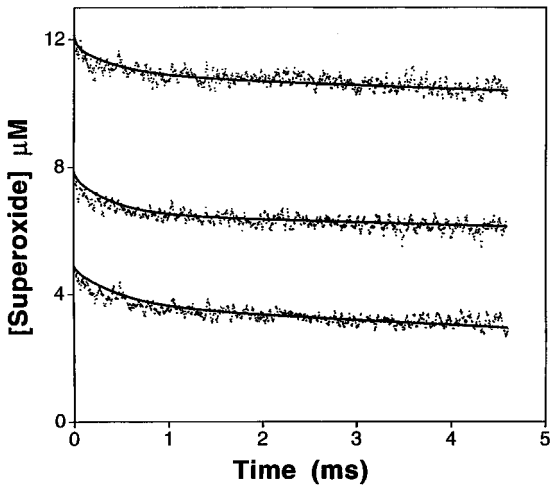

FIGURE 7: Superoxide decay catalyzed by Y34F human manganese superoxide dismutase as determined by pulse radiolysis. Data show the decrease in superoxide determined from its absorbance at 250 nm (ϵ = 2000 M^{-1} cm^{-1}). All solutions contained 0.5 μM Y34F MnSOD, 50 μM EDTA, 10 mM sodium formate, and 2.0 mM sodium pyrophosphate at pH 9.6 and 20 °C. Traces from the top of the figure down contained 12, 7.9, and 4.9 μM as initial concentrations of superoxide. The calculated lines shown in the figure are kinetic simulations (KINSIM), determined with the rate constants given in Table 3.

Table 3: Values of the Rate Constants for Catalysis by Wild-Type and Y34F Human Manganese Superoxide Dismutase[a]

rate constant	wild-type MnSOD	Y34F MnSOD
k_1 (M^{-1} s^{-1})	2×10^9	2×10^9
k_{-1} (s^{-1})	2×10^4	1×10^3
k_2 (s^{-1})	8×10^4	5×10^3
k_3 (M^{-1} s^{-1})	2×10^9	2×10^9
k_{-3} (s^{-1})	2×10^4	1×10^3
k_4 (s^{-1})	8×10^4	1×10^4
k_{-4} (M^{-1} s^{-1})	2×10^3	1×10^3
k_5 (s^{-1})	2×10^4	2×10^4
k_{-5} (s^{-1})	130	200

[a] Obtained by fitting the model of Scheme 1 using KINSIM (*37*) to the data for catalysis of the decay of superoxide. For Y34F hMnSOD the fit was to pulse radiolysis data measured at 20 °C and pH 9.6 under the conditions of Figure 7. The fit for wild-type MnSOD is from Hsu et al. (*8*) and was determined from pulse radiolysis data taken at 20 °C and pH 9.4.

Table 4: Values of the Steady-State Parameters for the Decay of Superoxide Catalyzed by Human MnSOD and Two Mutants

enzyme	k_{cat} (ms^{-1})	k_{cat}/K_m (μM^{-1} s^{-1})
wild-type MnSOD[a]	40	800
Y34F MnSOD[a]	3.3	870
Q143N MnSOD[b]	0.3	0.82

[a] Data for wild type (*8*) measured at 20 °C and pH 9.4 by pulse radiolysis; data for Y34F (this work) measured at 20 °C and pH 9.6 by pulse radiolysis. [b] Data obtained by stopped-flow spectrophotometry at 5 °C and pH 9.4 (*31*).

k_5 and k_{-5}, are quite similar to those for the wild type. Hence, the mutation Tyr 34 → Phe may be altering the inherent catalysis of superoxide decay and not the steps by which the inhibited complex is formed.

The value of k_{cat} for the mutant is about 10-fold less than for the wild type (Table 4), while the ratio k_{cat}/K_m is nearly identical for the two forms of MnSOD, near 10^9 M^{-1} s^{-1}, a value close to the diffusion-controlled limit. These values were obtained using the data of Table 3 and eqs 5−9 of Bull et al. (*13*). The results of Table 3 may not represent unique solutions to the appropriate kinetic equations for hMnSOD and mutants; however, they qualitatively represent trends in the catalytic pathway between the wild type and mutants of hMnSOD. Thus at low concentrations of superoxide compared with K_m (50 and 4 μM for the wild type and Y34F, respectively) the catalysis by these two enzymes is nearly identical, but near substrate saturation the mutant Y34F MnSOD is slower by 10-fold. This is consistent with a role for Tyr 34 in proton transfer, since it is at higher substrate concentrations that the enzyme needs rapid proton transfer to the active site and the maximal velocity of catalysis is expected to be proton-transfer-dependent in analogy with FeSOD (*35*). Perhaps Tyr 34 is itself a proton donor or through its participation in the hydrogen-bonded network is involved indirectly in proton donation required to dissociate hydrogen peroxide or the hydroperoxide anion HO_2^-. The crystal structure of Figure 3B shows that the hydrogen-bond chain from Tyr 34 and extending to the manganese-bound water is broken in the Y34F mutant. In the absence of this hydroxyl in Y34F there may be less proton donation to product peroxyl and maximal velocity (i.e., k_{cat}) is slowed. Certainly Y34F breaks the hydrogen-bond relay Mn(III)−hydroxyl−Gln 143−Tyr34−water−His 30. It is a reasonable assumption that proton-transfer steps are involved in k_4 (Scheme 1), and the data of Table 3 show a reduced value of k_4 in Y34F in comparison with the wild type.

Conclusions. Characterization of the structure, stability, and activity of Y34F hMnSOD provides insights into the functional role of the conserved Tyr 34 that impact our understanding of superoxide dismutase activity and metalloenzyme evolution. (*1*) The side-chain hydroxyl of the conserved residue Tyr 34 in MnSOD contributes to catalytic efficiency in MnSOD but is not essential at normal cellular superoxide concentrations. (*2*) The structure of the active site is unchanged by the replacement of Tyr 34 → Phe with the phenyl rings of Tyr 34 in the wild-type and Phe 34 in the mutant Y34F superimposable for two independent crystal forms of Y34F. (*3*) Y34F not only retains the wild-type active-site architecture but also shows a major increase in thermostability, arguing that Tyr 34 conservation is not due to a structural role. (*4*) The kinetic results suggest that the replacement Tyr 34 → Phe does not affect the diffusion-controlled steady-state constant k_{cat}/K_m, which has a value near 10^9 M^{-1} s^{-1} for both the wild-type and Y34F human MnSOD. (*5*) The replacement of Tyr 34 → Phe appears to affect the rate of maximal catalysis k_{cat}, reducing by about 10-fold the steps that determine k_{cat}. This and the breaking of the hydrogen-bonding chain at the active site caused by the replacement of Tyr 34 → Phe suggests that Tyr 34 is a proton donor or is involved indirectly by its hydrogen-bonded network to other residues and solvent for proton transfer. (*6*) The mutant Y34F shows enhanced product inhibition when compared with the wild type. This may be related to decreased proton transfer capability in the active site of the Y34F mutant. (*7*) Catalysis in the substrate-inhibited region by both Y34F and the wild type was not susceptible to enhancement by even up to 100 mM of buffer in solution, indicating that protonation from certain buffers in solution is not capable of enhancing the release of the inhibiting bound peroxide ion, as expected from the structurally sequestered nature of the MnSOD active site. (*8*) The combination of structural conservation, increased thermostability, and diffusion-controlled rate for Y34F under normal cellular superoxide levels prompts us to propose the hypothesis that conservation of active-site residues can reflect functional constraints from extreme rather than normal cellular conditions.

ACKNOWLEDGMENT

We thank Terence Lo, Hans Parge, Christopher Bruns, Yves Bourne, and Elizabeth Getzoff for discussions.

REFERENCES

1. Chance, B. Sies, H., and Boveris, A. (1979) *Phys. Rev. 59*, 527−605.
2. Borgstahl, G. E. O., Parge, H. E., Hickey, M. J., Beyer, W. F., Hallewell, R. A., and Tainer, J. A. (1992) *Cell 71*, 107−118.
3. Wagner, U. G., Pattridge, K. A., Ludwig, M. L., Stallings, W. C., Werber, M. M., Oefner, C., Frolow, F., and Sussman, J. L. (1993) *Protein Sci. 2*, 814−825.
4. Parker, M. W., and Blake, C. C. F. (1988) *J. Mol. Biol. 199*, 649−661.
5. Ludwig, M. L., Metzger, A. L., Pattridge, K. A., and Stallings, W. C. (1991) *J. Mol. Biol. 219*, 335−358.
6. Stoddard, B. L., Ringe, D., and Petsko, G. A. (1990) *Protein Eng. 4*, 113−119.
7. Cooper, J. B., McIntyre, K., Badasso, M. O., Wood, S. P., Zhang, Y., Garbe, T. R., and Young, D. (1995) *J. Mol. Biol. 246*, 531−544.
8. Hsu, J.-L., Hsieh, Y., Tu, C. K., O'Connor, D., Nick, H. S., and Silverman, D. N. (1996) *J. Biol. Chem. 271*, 17687−17691.
9. McCord, J. M., Boyle, J. A., Bay, E. D., Rizzolo, L. J., and Salin, M. L. (1977) in *Superoxide and Superoxide Dismutase* (Michelson, A. M., McCord, J. M., and Fridovich, I., Eds.) pp 129−138, Academic Press, London.
10. Getzoff, E. D., Cabelli, D. E., Fisher, C. L., Parge, H. E., Viezzoli, M. S., Banci, L., and Hallewell, R. A. (1992) *Nature 358*, 347−351.
11. McAdam, M. E., Fox, R. A., Lavelle, F., and Fielden, E. M. (1977) *Biochem. J. 165*, 71−79.
12. McAdam, M. E., Lavelle, F., Fox, R. A., and Fielden, E. M. (1977) *Biochem. J. 165*, 81−97.

13. Bull, C., Niederhoffer, E. C., Yoshida, T., and Fee, J. A. (1991) *J. Am. Chem. Soc. 113*, 4069−4076.
14. Lah, M. S., Dixon, M. M., Pattridge, K. A., Stallings, W. C., Fee, J. A., and Ludwig, M. L. (1995) *Biochemistry 34*, 1646−1660.
15. Hunter, T., Ikebukuro, K., Bannister, W. H., Bannister, J. V., and Hunter, G. J. (1997) *Biochemistry 36*, 4925−4933.
16. Sorkin, D. L., and Miller, A.-F. (1997) *Biochemistry 36*, 4916−4924.
17. Beck, Y., Oren, R., Amit, B., Levanon, A., Gorecki, M., and Hartman, J. R. (1987) *Nucleic Acids Res. 15*, 9076.
18. Beck, B. A., Bartfield, D., Yavin, Z., Levanon, A., Gorecki, M., and Hartman, J. R. (1988) *Bio/Technology 6*, 930−935.
19. Borgstahl, G. E. O., Parge, H. E., Hickey, M. J., Johnson, M. J., Boissinot, M., Hallewell, R. A., Lepock, J. R., Cabelli, D. E., and Tainer, J. A. (1996) *Biochemistry 35*, 4287−4297.
20. Brünger, A. T., Kuriyan, J., and Karplus, M. (1987) *Science 235*, 458−460.
21. Otwinowski, Z., and Minor, W. (1997) in *Methods in Enzymology* (Carter, C. W., Jr., and Sweet, R. M., Eds.) Vol. 276, pp 307−326, Academic Press, New York.
22. Read, R. J. (1986) *Acta Crystallogr. A42*, 140−149.
23. McRee, D. E. (1992) *J. Mol. Graphics 10*, 44−46.
24. Jiang, J.-S., and Brünger, A. T. (1994) *J. Mol. Biol. 243*, 100−115.
25. Navaza, J. (1994) *Acta Crystallogr. A50*, 157−163.
26. Borgstahl, G. E. O., Rogers, P. H., and Arnone, A. (1994) *J. Mol. Biol. 236*, 817−830.
27. Sturtevant, J. M. (1987) *Annu. Rev. Phys. Chem. 38*, 463−488.
28. Schwarz, H. A. (1981) *J. Chem. Educ. 58*, 101−105.
29. Rabani, J. and Nielson, S. O. (1969) *J. Phys. Chem. 73*, 3736−3744.
30. Ramachandran, G. N., and Sasisekharan, V. (1968) in *Advances in Protein Chemistry* (Anfinsen, C. B., Jr., Anson, M. L., Edsall, J. T., and Richards, F. M., Eds.) Vol. 23, pp 283−438, Academic Press, New York.
31. Hsieh, Y., Guan, Y., Tu, C., Bratt, P. J., Angerhofer, A., Lepock, J. R., Hickey, M. J., Tainer, J. A., Nick, H. S., and Silverman, D. N. (1998) *Biochemistry 37*, 4731−4739.
32. Lepock, J. R., Ritchie, K. P., Kolios, M. C., Rodahl, A. M., Heinz, K., and Kruuv, J. (1992) *Biochemistry 31*, 12706−12712.
33. Privalov, P. L. and Khechinashvili, N. N. (1974) *J. Mol. Biol. 86*, 665−684.
34. Shoichet, B. K., Baase, W. A., Kuroki, R., and Matthews, B. W. (1995*) Proc. Natl. Acad. Sci. U.S.A. 92*, 452−456.
35. Bull, C., and Fee, J. A. (1985) *J. Am. Chem. Soc. 107*, 3295−3304.
36. Whittaker, M. M., and Whittaker, J. W. (1997) *Biochemistry 36*, 8923−8931.
37. Barshop, B. A., Wrenn, R. F., and Frieden, C. (1983) *Anal. Biochem. 130*, 134−145.
38. Carson, M. (1991) *J. Appl. Crystallogr. 24*, 958−961.

BI972394L